Takano, T., & Dickerson, R. E. (1981a) *J. Mol. Biol. 153*, 79–94.
Takano, T., & Dickerson, R. E. (1981b) *J. Mol. Biol. 153*, 95–115.
Trewhella, J., Carlson, V. A. P., Curtis, E. H., & Heidorn, D. B. (1988) *Biochemistry 227*, 1121–1125.
Ulmer, D. D., & Kagi, J. H. R. (1968) *Biochemistry 7*, 2710–2717.
Venyaminov, S. Y., & Kalnin, N. N. (1990) *Biopolymers 30*, 1243–1257.
Wand, J. A., Rober, H., & Englander, S. W. (1986) *Biochemistry 25*, 1107–1114.
Watt, G. D., & Sturtevant, J. M. (1969) *Biochemistry 8*, 4567–4571.
Weber, C., Michel, B., & Bosshard, H. R. (1987) *Proc. Natl. Acad. Sci. U.S.A. 84*, 6687–6691.
Yang, P. W., Mantsch, H. H., Arrondo, J. L. R., Saint-Girons, I., Guillou, Y., Cohen, G. N., & Barzu, O. (1987) *Biochemistry 26*, 2706–2711.
Yang, W.-J., Griffiths, P. R., Byler, D. M., & Susi, H. (1985) *Appl. Spectrosc. 39*, 282–287.
Yashi, S. C., Keiderling, T. A., Bonora, G. M., & Toniolo, C. C. (1986) *Biopolymers 25*, 79–89.

Electron Spin Echo Envelope Modulation Spectroscopic Study of Iron–Nitrogen Interactions in Myoglobin Hydroxide and Fe(III) Tetraphenylporphyrin Models†

Richard S. Magliozzo*,‡ and Jack Peisach‡,§

Department of Molecular Pharmacology and Department of Physiology and Biophysics, Albert Einstein College of Medicine of Yeshiva University, Bronx, New York 10461

Received June 17, 1991; Revised Manuscript Received September 26, 1991

ABSTRACT: The electron–nuclear coupling in low-spin iron complexes including myoglobin hydroxide (MbOH) and two related model compounds, Fe(III) tetraphenylporphyrin(pyridine)(OR^-) (R = H or CH_3) and Fe(III) tetraphenylporphyrin(butylamine)(OR^-) was investigated using electron spin echo envelope modulation (ESEEM) spectroscopy. The assignment of frequency components in ESEEM spectra was accomplished through the use of nitrogen isotopic substitution wherever necessary. For example, the proximal imidazole coupling in MbOH was investigated without interference from the contributions of porphyrin ^{14}N nuclei after substitution of the heme in native Mb with ^{15}N-labeled heme. Computer simulation of spectra using angle selected techniques enabled the assignment of parameters describing the hyperfine and quadrupole interactions for axially bound nitrogen of imidazole in MbOH, of axial pyridine and butylamine in the models, and for the porphyrin nitrogens of the heme in native MbOH. The isotropic component of axial nitrogen hyperfine interactions exhibits a trend from 5 to 4 MHz, with imidazole (MbOH) > pyridine > amine. The nuclear quadrupole interaction coupling constant e^2Qq was near 2 MHz for all nitrogens in these complexes. The Q_{zz} axis of the nuclear quadrupole interaction tensor for the proximal imidazole nitrogen in MbOH was found to be aligned near g_z (g_{max}) in MbOH, suggesting that g_z is near the heme normal. A crystal field analysis, that allows a calculation of rhombic and axial splittings for the d orbitals of the t_{2g} set in a low-spin heme complex, based on the g tensor assignment $g_z > g_y > g_x$, yielded results that are consistent with the poor π-acceptor properties expected for the closed shell oxygen atom of the hydroxide ligand in MbOH. A discussion is presented of the unusual results reported in a linear electric field effect in EPR (LEFE) study of MbOH published previously [Mims, W. B., & Peisach, J. (1976) *J. Chem. Phys. 64*, 1074–1091].

An understanding of the chemistry of the prosthetic group and its axial ligands in heme proteins has often been provided by magnetic resonance spectroscopic studies. For example, ESEEM[1] spectroscopy, a pulsed EPR technique that directly probes the interactions between unpaired electrons and nearby nuclei of ^{14}N-containing ligands has been used to study the axial ligation in various low-spin heme protein complexes (Peisach et al., 1979; Magliozzo et al., 1987). The approach to this type of investigation involved comparisons between protein and iron porphyrin or heme model complexes, a technique that remains especially useful because models containing different axial ligands can be readily prepared. A complete quantitative analysis of the electron–nuclear couplings in some of those systems, however, was not possible because of the need to simultaneously assign parameters, including those for the nuclear Zeeman, hyperfine, and quadrupole interactions, for both axial and equatorial ligand nitrogens. A method involving isotopic substitution can sometimes be used to assign the spectral contributions of the various ligands. For example, substitution of ^{15}N for ^{14}N in the histidines of yeast cytochrome *c* oxidase (Martin et al., 1985) was used to simplify the spectra in an ENDOR study to identify the axial ligands to the heme. Isotopic substitution of the native prosthetic group in a heme protein by recon-

† This work was supported by Grants GM-40168 and RR-02583 from the National Institutes of Health.
* Author to whom correspondence should be addressed.
‡ Department of Molecular Pharmacology.
§ Department of Physiology and Biophysics.

[1] Abbreviations: ESEEM, electron spin echo envelope modulation; ENDOR, electron–nuclear double resonance; TPP, tetraphenylporphyrin; Hb, hemoglobin, Mb, myoglobin; LEFE, linear electric field effect; nqi, nuclear quadrupole interaction; nqr, nuclear quadrupole resonance; pyr, pyridine.

0006-2960/92/0431-189$03.00/0

stitution with a ^{15}N-substituted heme is another simplifying approach utilized here.

Methods for the analysis of ESEEM spectra using angle selected simulation techniques have recently been applied to the quantitative treatment of electron–nuclear couplings in copper–nitrogen systems (Cornelius et al., 1990). For low-spin iron complexes, an accurate determination of anisotropic hyperfine coupling interactions can potentially be achieved since data can be simulated at various positions along the rhombic EPR absorption spectrum of the species of interest. This report concerns the application of ESEEM spectroscopy and spectral simulation techniques to the study of low-spin heme and Fe(III) TPP complexes containing nitrogen and oxygen axial ligand pairs, including myoglobin hydroxide. A high-spin analogue of these structures, aquo-metHb was the subject of a detailed single-crystal ENDOR study (Scholes et al., 1982) in which the hyperfine and quadrupole couplings for all the nitrogen ligands of iron were reported. Iron–nitrogen couplings for some low-spin heme protein and model complexes were reported in ENDOR studies performed on frozen solution samples (Mulks et al., 1979; Scholes et al., 1986), though MbOH was not included in those investigations. The analysis of ENDOR spectra for complexes such as MbN_3^- (Mulks et al., 1979) was limited in scope because of the multiplicity of nitrogen interactions, and, therefore, no analysis of the proximal imidazole coupling was made.

The complexes studied here were chosen first of all because the analysis of couplings for a single axially coordinated nitrogen is straightforward compared to the identification and analysis of the couplings for low-spin forms containing additional nitrogen in axial azide or cyanide ligands. Though the models that contain axially bound pyridine or butylamine do not have exact biological analogues, they were useful in understanding the ESEEM spectra of MbOH. The interpretation of data here was greatly simplified through the use of [^{15}N]TPP, [^{15}N]pyridine, and myoglobin reconstituted with [^{15}N]heme. A second reason for the choice of MbOH for this study concerns the orientation of the g tensor in this species. The results of LEFE in EPR experiments published previously (Mims & Peisach, 1976) were consistent with a g tensor axis system in MbOH that differed from that in other low-spin forms. A comparison of hyperfine and quadrupole interaction parameters associated with the iron–nitrogen couplings in MbOH to the parameters for other forms was therefore expected to reveal differences that resulted from the unusual g tensor. The ^{14}N nuclear quadrupole interaction parameters for axial nitrogen were of special interest since these provide information about the direction of the nitrogen lone pair donor orbital in relation to the magnetic and molecular axes.

Another aim addressed here in a preliminary way concerns whether the analysis of axial couplings could reveal a distinction between amino and imino ligands in low-spin heme complexes. Results of such an experiment are relevant to the identity of axial ligands in cytochrome *f*, for example, in which an amine is believed to be a heme ligand (Siedow et al., 1980; Rigby et al., 1988).

This report provides a foundation upon which the study of axial ligand effects in other low-spin derivatives and other heme proteins will be extended in the future.

Materials and Methods

Myoglobin Hydroxide. Horse Mb (Sigma) was used without further purification. It was converted to apomyoglobin (Teale, 1959) and was reconstituted with [^{15}N]heme (generously provided by Kevin Smith) according to a published procedure (Ascoli et al., 1981) with minor modifications. The reconstituted [^{15}N]heme metMb was concentrated to approximately 3 mM by ultrafiltration. The hydroxide forms of the reconstituted Mb and native Mb were prepared by adjusting the pH of aliquots of the protein solutions to pH 11.2, using KOH. The titration process was accomplished very quickly, and the resultant red solutions were immediately frozen in liquid nitrogen, since incubation at high pH rapidly generates denatured forms of the protein. The integrity of the MbOH samples was established by conventional EPR spectroscopy from which the sample composition was estimated to be 90% MbOH (Gurd et al., 1967) (observed g values = 2.55, 2.14, and 1.83) with the remainder composed of a second low-spin species and a small amount of high-spin metMb. The minority species were present in concentrations too low to interfere with spin echo measurements.

Model Complexes. The Fe(III) [^{15}N]TPP(butylamine)(OR^-) complex was prepared by dissolving Fe(III) [^{15}N]TPPCl (Porphyrin Products, Logan, UT) in toluene followed by the addition of a solution of butylamine containing 10% methanol to give 10 mM Fe(III) [^{15}N]TPP, 200 mM butylamine, and 50 mM methanol. The EPR spectrum of this complex (77 K) had g values typical of low-spin iron porphyrins with nitrogen/oxygen axial ligand combinations (g = 2.49, 2.16, and 1.89) (Gurd et al., 1967; Tang et al., 1976; Ainscough et al., 1978). A complex with the same EPR spectrum was produced in solutions of the iron porphyrin and the amine plus 1% [*tert*-butylammonium hydroxide (1 M) in methanol]. Similar complexes were prepared using Fe(III) [^{14}N]- or [^{15}N]TPPCl with [^{15}N]- or [^{14}N]pyridine plus *tert*-butyl ammonium hydroxide in methanol. Final concentrations were 10 mM Fe(III) TPP, 10 mM pyridine, 0.6 mM methanol, and 20 mM *tert*-butylammonium hydroxide (g = 2.47, 2.14, and 1.91). Whether the sixth ligand is actually hydroxide or methoxide in the model complexes is not known and OR^- is used to indicate this species.

Spectroscopy. Continuous wave EPR spectra were recorded with a Varian E-112 spectrometer equipped with a Systron–Donner frequency counter and a Varian NMR Gaussmeter. The pulsed EPR spectrometer used to obtain electron spin echo envelope data at liquid helium temperatures has been described elsewhere (McCracken et al., 1987). It employs a reflection cavity system with a folded stripline resonant element (Lin et al., 1985) and a coupling scheme suited for use in a cryogenic immersion Dewar (Britt & Klein, 1987). Samples were contained in conventional 4-mm (o.d.) EPR tubes, enabling the characterization of each preparation by continuous wave EPR spectroscopy.

As in previous ESEEM studies, electron spin echo envelopes were obtained using the three-pulse or "stimulated echo" method (Peisach et al., 1979; Mims & Peisach, 1979a) and were generally recorded at three or more magnetic field settings. The value of τ, the time interval between the first two pulses, was chosen to suppress the modulation that occurs at the Larmor frequency of hydrogen nuclei (Peisach et al., 1979). Data were extrapolated to "zero time" and Fourier transformed (Mims, 1984) in order to obtain the spectra presented throughout this work.

Simulations. Simulation of spectra (Cornelius et al., 1990) was accomplished using angle selected methods applied by Hurst et al. (1985) for generating ENDOR spectra, and a formalism described previously for the simulation of stimulated echo envelope modulation functions (Mims, 1972). For an EPR species that exhibits large g anisotropy, such as the low-spin iron porphyrin complexes, only a specific set of molecular orientations are resonant at the experimental magnetic

field setting H_0 (Riste & Hyde, 1969). The g tensors for the complexes of interest are used to calculate the selected molecular orientations as the first step in the simulation of an ESEEM spectrum. Simulations were usually generated as the sum of spectra at 10 different field positions centered at the experimental H_0 and spanning 10–20 Gauss. A better approximation of experimental conditions was achieved by this approach as the width of the microwave pulse, H_1, is incorporated into the simulation. However, all the information required to evaluate the fit of simulation to spectra was contained in a simulation at the experimental field only.

In the description by Hurst et al. (1985) for copper complexes, both the g tensor and the metal nuclear hyperfine interaction are considered in the calculation of molecular orientations. Since $I = 0$ for the normally occurring iron isotope, no metal hyperfine interaction is involved here. Note also that only the g tensor is utilized in calculating orientations without consideration of contributions from the ligand hyperfine interactions, which are negligibly small (approximately 2 Gauss).

Parameters describing the ligand hyperfine interaction and the orientation of its principal axis system relative to the g tensor, and the parameters for the ^{14}N nuclear quadrupole interaction are refined essentially by trial and error. Three ligand hyperfine matrix elements, estimated from the position of the highest frequency ^{14}N component seen in the ESEEM spectra (see results), are assigned to A_x, A_y, and A_z, (or A_1, A_2, and A_3) to achieve the proper field dependence of these lines at three experimental g values. The principal axis orientation is then determined in the frame of the g tensor. This method, used for the simulation of spectra for the axial nitrogen coupling in MbOH, was abbreviated in other cases for which no rotation angles were determined. In these cases, A_1, A_2, $A_3 = A_x$, A_y, A_z.

The nuclear quadrupole parameters to be assigned include e^2Qq, the nuclear quadrupole coupling constant, η, the asymmetry parameter, and the Euler angles α, β, γ, describing the relative orientation of the nqi principal axis system with respect to the g tensor. Other parameters in simulations concern a choice of conditions for presentation of the time domain simulation in the frequency domain. The line widths of components in the Fourier-transformed simulations arise in part from an exponential decay function applied to the time domain functions (Cornelius et al., 1990).

Simulations were only begun after the identification of the origin of frequency components observed in an ESEEM spectrum was made. In general, the assignment of a component to a particular nucleus could be made by correlating its frequency vs field dependence with the magnitude of Zeeman interactions for various nuclei. Such a procedure is more straightforward for an $I = 1/2$ nucleus such as ^{15}N than it is for ^{14}N ($I = 1$), especially when the hyperfine coupling is anisotropic, and is difficult because the weak Zeeman interaction for ^{14}N gives frequency changes on the order of only tenths of MHz for a 1-kG change in magnetic field. Furthermore, the complexity of heme protein spectra containing contributions from several nitrogens presents an additional difficulty due to the multiplicity of similar nuclei coupled to the same spin system. Therefore, through substitution of ^{14}N sites using ^{15}N-labeled ligands, a more direct approach to the identification and analysis of pyrrole and axial nitrogen couplings in ESEEM spectra was possible.

Results and Discussion

Axial Nitrogen Coupling. Figure 1A (top panel) shows the ESEEM spectrum of the model complex Fe(III) TPP(pyr)-

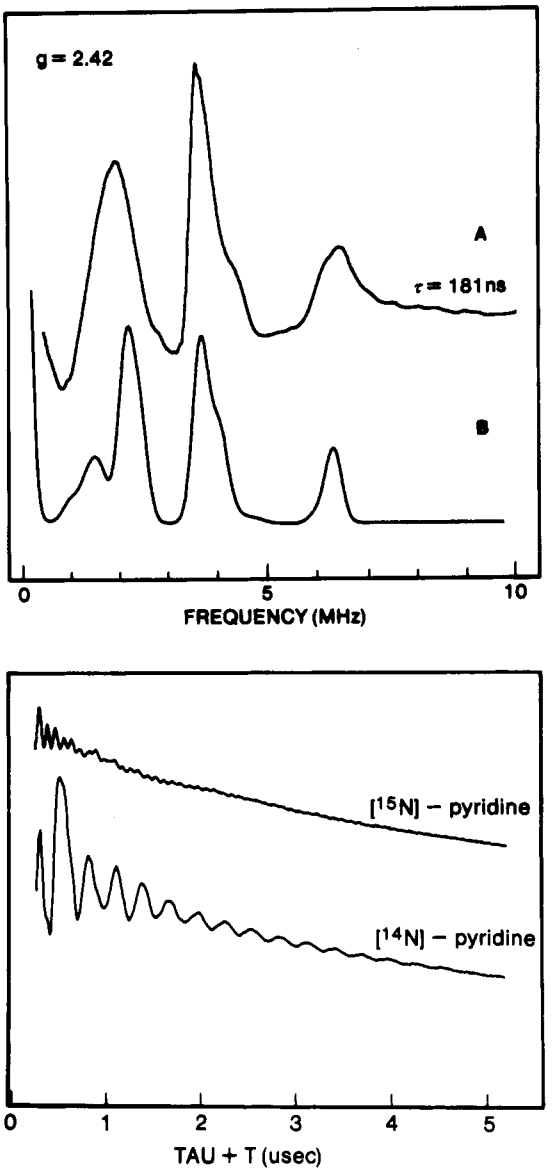

FIGURE 1: (Top, spectrum A) ESEEM spectrum of the low-spin complex Fe(III) [^{15}N]TPP([^{14}N]pyridine)(OR^-). Experimental conditions: frequency, 8.8135 GHz; magnetic field, 2600 Gauss; pulse power, 70 W. (Spectrum B) Fourier transform of ESEEM simulation for the axially coordinated imino nitrogen of [^{14}N]pyridine. Simulation parameters: A_x, A_y, A_z = 4.7, 5.1, 4.1 MHz; e^2Qq = 2.8 MHz; η = 0.5; nqi Euler angles α, β, γ = 0°, 13°, 0°. (Bottom) Three-pulse spin echo envelopes for Fe(III) [^{15}N]TPP([^{15}N]pyridine)(OR^-) and Fe(III) [^{15}N]TPP([^{14}N]pyridine)(OR^-) τ = 181 ns. Experimental conditions ([^{15}N]pyridine data): frequency, 8.7832 GHz; field, 2600 G; power, 40 W; ([^{14}N]pyridine data) frequency, 8.8135 GHz; field 2600 G; power, 70 W. The echo amplitudes were close to equal in these two data sets.

(OR^-), prepared with [^{15}N]TPP and [^{14}N]pyridine, and a simulation of the spectrum, at g = 2.42. A discussion of the simulation parameters appears below. Additional data sets (not shown) were recorded at other values of τ, and at g = 2.19 and 1.90, where simulations were also satisfactory using the parameters summarized in Table I. The bottom panel of Figure 1 shows the time domain ESEEM data for the [^{15}N]TPP complex prepared with [^{15}N]- or [^{14}N]pyridine, which were examined to determine if contributions from ^{15}N nuclei interfered with the assignment of ^{14}N modulations. The data for the fully ^{15}N-substituted complex contains some shallow modulation components and a component whose periodicity (90 ns) corresponds to the proton Larmor frequency (~11 MHz). The shallow modulations give rise to broad

Table I: Hyperfine and Quadrupole Coupling Parameters

	hyperfine coupling (MHz)				quadrupole coupling (MHz)	
	A_1	A_2	A_3	a_{iso}[a]	e^2Qq	η[b]
A. Axially Coordinated Nitrogens in Model Complexes and in MbOH						
Fe(III) [^{15}N]TPP(pyridine)(OR^-)	4.7[c]	5.1	4.1	4.6	2.8 (α, β, γ = 0°, 13°, 0°)	0.5
Fe(III) [^{15}N]TPP(butylamine)(OR^-)	4.0[c]	4.4	3.5	4.0	2.5 (α, β, γ = 0°, 9°, 0°)	0.4
MbOH ([^{15}N]heme)	5.5 (α, β, γ = 26°, 15°, 0°)	5.5	4.2	5.1	2.3 (α, β, γ = 0°, 13°, 0°)	0.1
B. Porphyrin Nitrogens						
Fe(III) [^{14}N]TTP([^{15}N]pyridine(OR^-)	4.6[c]	5.1	4.9	4.9	2.2 (α, β, γ = 0°, 48°, 0°)	0.2
MbOH	4.9[c]	5.1	5.3	5.1	2.2 (α, β, γ = 0°, 45°, 0°)	0.1

[a] $a_{iso} = 1/3[A_1 + A_2 + A_3]$. [b] $\eta = (q_{yy} - q_{xx})/q_{zz}$. [c] Hyperfine and g tensor axes were taken to be collinear, $A_1 = A_x$, $A_2 = A_y$, and $A_3 = A_z$.

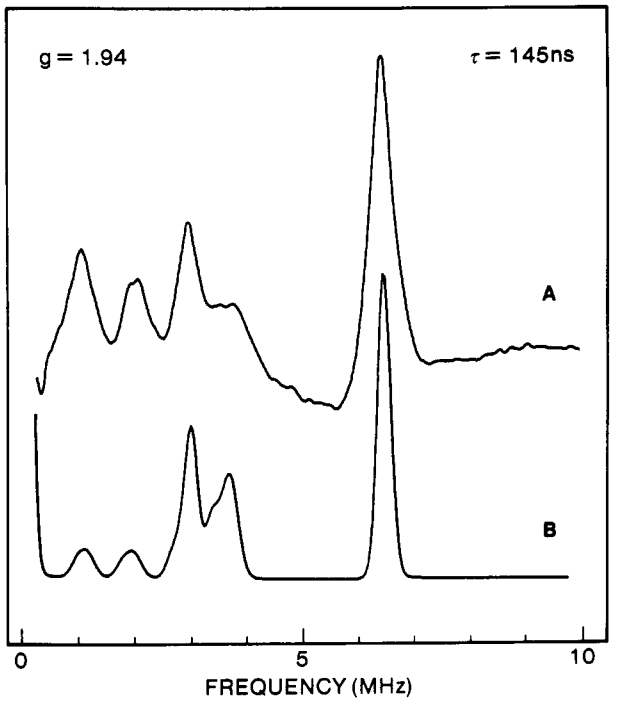

FIGURE 2: (A) ESEEM spectrum of the low-spin complex Fe(III) [^{15}N]TPP([^{14}N]butylamine)(OR^-). Experimental conditions: frequency, 8.8627 GHz; magnetic field, 2600 Gauss; pulse power, 40 W. (B) Fourier transform of ESEEM simulation for the axially coordinated amino nitrogen of [^{14}N]butylamine. Simulation parameters: A_x, A_y, A_z = 4.0, 4.4, 3.5 MHz; e^2Qq = 2.5 MHz; η = 0.4; nqi Euler angles α, β, γ = 0°, 9°, 0°.

peaks in Fourier transforms of data for the all ^{15}N sample (not shown), none of which appears above the noise level in spectra from samples containing [^{14}N]TPP or [^{14}N]pyridine. Therefore, the frequency components seen in the Fourier transform for the complex containing [^{15}N]TPP and [^{14}N]-pyridine all arise from the coupling to the single axially bound ^{14}N. The interpretation of data for other complexes prepared with ^{15}N-labeled ligands is simplified by the hypothesis that ^{15}N-coupling components are too shallow to give significant peak intensity in the ESEEM spectra.

Figure 2 shows an ESEEM spectrum and a simulation for Fe(III) [^{15}N]TPP(butylamine)(OR^-) at g = 1.94. The spectrum differs from that shown in Figure 1 in part because of the difference in experimental field setting. The spectrum of the butylamine complex at g = 2.4 (not shown) closely resembles the pyridine spectrum at the same g value, though the lines are shifted to lower frequency by about 1 MHz.

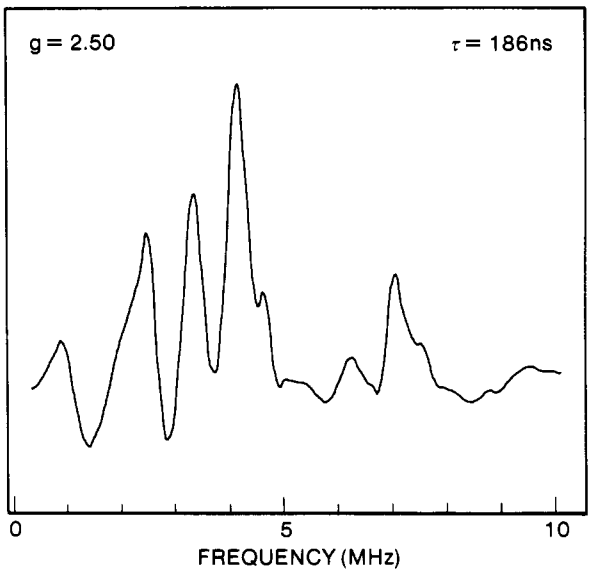

FIGURE 3: ESEEM spectrum of native MbOH. Experimental conditions: frequency, 8.8522 GHz; field, 2532 G; power, 60 W.

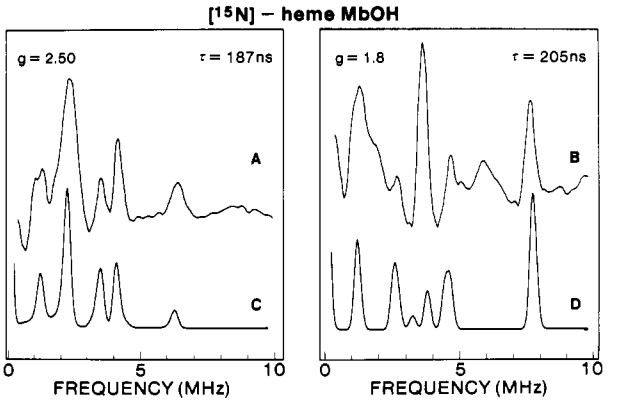

FIGURE 4: (A, B) ESEEM spectra of [^{15}N]heme MbOH. Experimental conditions: (A) frequency, 8.8291 GHz; magnetic field, 2525 Gauss; pulse power, 80 W; (B) frequency, 8.8163 GHz; magnetic field, 3440 Gauss; pulse power, 80 W. (C, D) Fourier transforms of ESEEM simulations for the directly coordinated imidazole nitrogen in [^{15}N]heme MbOH. Simulation parameters: A_1, A_2, A_3 = 5.5, 5.5, 4.2 MHz with hyperfine Euler rotation angles α, β, γ = 26°, 15°, 0°; e^2Qq, 2.3 MHz; η, 0.1; nqi Euler angles α, β, γ = 0°, 13°, 0°. The broad feature near 6 MHz in spectrum B is an artifact.

Figure 3 shows an ESEEM spectrum for a sample of MbOH prepared from native myoglobin. No direct assignment of the components could be made before eliminating or identifying the contribution of the pyrrole nitrogens. A

[^{15}N]heme-substituted myoglobin sample provided the means to directly select the axial coupling components. Figure 4 shows two spectra with simulations for [^{15}N]heme MbOH at $g = 2.5$ and 1.8. The spectrum of the protein at $g = 2.5$ is similar to that at $g = 2.42$ for the model containing [^{14}N]-pyridine (Figure 1, top). The simulation of the protein spectrum at $g = 1.8$ is not as good as that for the low-field spectrum if one considers the relative intensities of the lines. A simulation of the components as they would appear in a continuous wave experiment (not shown), i.e., without an assignment of τ, showed a more accurate ratio of intensities for the 3.8- and 7.8-MHz peaks. This result is not clearly understood at this time, and the "τ" effects in simulations do not always correspond very well with the suppression and enhancement effects seen experimentally.

The lines appearing in spectra for the protein and the models containing [^{14}N]pyridine or butylamine correspond to modulation frequencies arising from the coupling of the axial nitrogen nuclear spin, $I = 1$, to the $S = 1/2$ electron spin of Fe(III). This assignment follows directly from inspection of the spectra for the [^{15}N]- and [^{14}N]pyridine-containing samples and from the similarities in spectra of the pyridine complex and the amine or imidazole (MbOH) complexes. The conclusion that the frequencies arise from the *directly* coordinated nitrogen of the proximal imidazole in the protein and not the remote nitrogen [as would be expected in a typical Cu(II) imidazole complex (Mims & Peisach, 1978)] is drawn by noting that the spectrum of the pyridine model complex is similar to that of [^{15}N]heme MbOH, the most obvious similarity being the appearance of the highest frequency peak near 6 MHz in spectra recorded at low field. This component arises from the nitrogen nuclear transition for which $\Delta m_I = 2$ occurring in the electron spin manifold in which the nuclear hyperfine interaction adds to the Zeeman interaction. Its frequency corresponds to a value expected for a coupling of approximately 5 MHz (see below). Since the imino nitrogens of both imidazole and pyridine should have similar coupling interactions, the remote nitrogen of imidazole would be too weakly interacting to give rise to modulations in these ESEEM spectra. For example, the remote nitrogen site of the imidazole ligands in the copper protein stellacyanin is coupled $\sim$1/20th as strongly as the directly coordinated nitrogen (Roberts et al., 1980; Mims & Peisach, 1979b).

The frequencies and intensities of the lines in the ESEEM spectra depend on the magnitudes of the ligand nuclear Zeeman, hyperfine, and quadrupole interactions as well as on the orientation of the principal axis systems of the hyperfine and quadrupole tensors with respect to the g tensor. A rough estimate of coupling parameters can be made by application of the first-order frequency expression useful for analysis of continuous wave ENDOR spectra. For a case in which good resolution of multiple components is found (as for MbOH at $g = 2.5$) and when hyperfine and quadrupole axes are colinear with the g tensor (and when the experimental field is aligned with a principal axis), the observed ESEEM frequencies should be given by

$$\nu = 1/2A_{zz} \pm \nu(^{14}\mathrm{N}) \pm 3/2Q_{zz}$$

where A_{zz} is the z component of the nitrogen nuclear hyperfine interaction, Q_{zz} is the z component of the ^{14}N nuclear quadrupole tensor, and ν is the ^{14}N nuclear Larmor frequency. The expression predicts four lines disposed about the value $1/2A_{zz}$ with pairs split by $2\nu(^{14}\mathrm{N})$. Each line of either pair corresponds to a nuclear transition occurring in different electron spin state manifolds. The set of coupling parameters used to simulate the $g = 2.5$ data for [^{15}N]heme MbOH gives the components

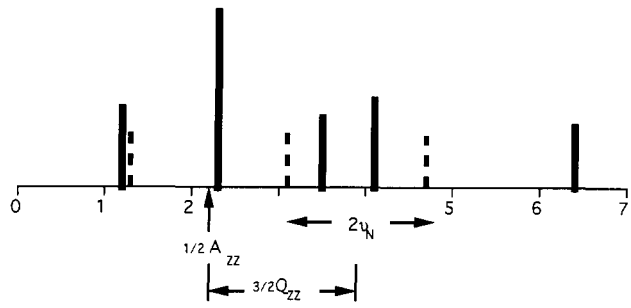

FIGURE 5: Stick spectra showing the frequency components from the ESEEM spectrum of [^{15}N]heme MbOH (solid lines) at $g = 2.5$ and the frequency components given by the expression for ENDOR spectra, calculated using $A_{zz} = 4.3$ MHz and $e^2Qq = 2.1$ MHz ($Q_{zz} = 1/2e^2Qq$) (dashed lines). A simulation of the MbOH ESEEM data appears in Figure 4, spectrum C.

occuring at 4.7, 3.1, 1.2, and −0.4 MHz (Figure 5, dashed lines). The lines at 3.5 and 6.4 MHz in the MbOH data occurring at the sum of (1.2 + 2.3 MHz) and (2.3 + 4.1 MHz) are so-called double-quantum transition frequencies appearing in the ESEEM spectra because of the excitation of partially forbidden transitions (Mims & Peisach, 1979a). These lines are usually not seen in ENDOR spectra. The highest frequency line appears at approximately $2[\nu(^{14}\mathrm{N}) + 1/2A_{zz}]$, allowing an estimate of the z component of the hyperfine coupling to be readily made. (The position of this line is not strongly dependent on the quadrupole coupling parameters, though its position and shape vary with the rotation of the hyperfine principal axis systems with respect to the g tensor). An estimate of Q_{zz} ($1/2e^2Qq$) can be made by noting that the spacing between the value of $1/2A_{zz}$ and the midpoint of the pair of lines at 2.95 and 4.55 MHz [those given by $1/2A_{zz} + 3/2Q_{zz} - \nu(^{14}\mathrm{N})$ and $1/2A_{zz} + 3/2Q_{zz} + \nu(^{14}\mathrm{N})$] gives $3/2Q_{zz}$. The diagram illustrates that the first-order ENDOR expression does not give a reasonable match of components to the data using the couplings that give an excellent simulation at g_z. The strong dependence of the frequencies on the angle β, for example, renders the usefulness of the first-order expression limited, though estimates for quadrupole and hyperfine coupling can be obtained and certainly the trends in hyperfine coupling in ESEEM spectra can be readily understood by inspection of the position of the highest frequency ESEEM line.

For an accurate determination of coupling parameters and to explore the axis orientations, angle selected methods were used to calculate the simulations presented. A difficulty in the assignment of simulation parameters involves the choice of axis labels for the observed g values, since no single-crystal EPR data are available for the complexes of primary interest here. The g tensor axes in the molecular framework of a low-spin heme complex have been assigned for crystalline MbN_3^-, in which g_z is found near the heme normal and corresponds to g_{max}; g_y and g_x lie in the heme plane nearly passing through the meso carbon positions (Helcke' et al., 1968; Hori, 1971), and g_x (Helcke' et al., 1968) lies nearly along the projection onto the heme of the proximal imidazole plane. The experimentally observed g values for the heme complexes studied here were tentatively assigned such that $g_z > g_y > g_x$. [An alternate arrangement ($g_x > g_y > g_z$) will be discussed below.] A more rigorous assignment of g tensor axes in these complexes can be made in the following way.

The "lone pair" donor orbital of the axial nitrogen ligands should be directed close to the heme normal in order to form a σ bond to iron. The heme normal will then correspond to the direction of the principal axis of the nqi tensor, usually Q_{zz}, occurring along the nitrogen lone pair orbital. The tensor

element along this axis represents the largest value of the electric field gradient. The angle between this axis and g_z is described by an Euler rotation angle β, which in all simulations for axial ligands was found to be $\leq 13°$. Therefore, this angle allows the localization of the z molecular axis (see below).

The hyperfine and quadrupole parameters for axial nitrogen couplings are summarized in Table I for the model complexes and for [^{15}N]heme MbOH. The elements of the hyperfine coupling matrix were readily approximated, using estimated nqi parameters, since the high-frequency components in simulations were sensitive to the values of A_1, A_2, and A_3, at various experimental field settings. For the protein, the principal elements of the hyperfine matrix were adjusted, along with the angles that describe the relative orientation of the hyperfine axis system and the g tensor [for example, the A_3 axis rotates through the Euler angle β onto g_z (Gurbiel et al., 1989)], to achieve satisfactory simulation of spectra at three magnetic field settings. All other parameters were finally adjusted to achieve the best simulation, determined by eye, of the intensity and frequency of all components. For [^{15}N]heme MbOH, this procedure resulted in an axially symmetric hyperfine matrix with a small anisotropy (−0.9, 0.4, and 0.4 MHz for A_3, A_2, and A_1, respectively) and small deviations from colinearity of the g and hyperfine tensors (see Table I). For the model complexes, the hyperfine tensors were considered to be colinear with the g tensors to simplify the procedure of fitting simulations to spectra at g values away from the extrema of the EPR absorption.[2] This approximation is reasonable given the small anisotropy of this coupling.

The hyperfine coupling terms give an isotropic (Fermi contact) coupling value of 5.1 MHz for the proximal imidazole in MbOH [$a_{iso} = 1/3[A_3 + A_2 + A_1)$]. The related isotropic couplings in the model complexes were 4.6 and 4.0 MHz for the pyridine and butylamine axial ligands, respectively. These couplings are smaller than those reported for the proximal imidazole nitrogen in high-spin metHb (9.3 MHz) (Scholes et al., 1982) and are nearer to the value of 5.6 MHz for the imidazole nitrogen in the low-spin complex Fe(III) TPP(imidazole)$_2$ (Scholes et al., 1986).[3] In an earlier ESEEM study (Peisach et al., 1979), the hyperfine coupling to pyridine nitrogen in the low-spin complex heme(pyridine)(2-mercaptoethanol) was estimated to be ≈2 MHz and was also ≈2 MHz for the axial nitrogen in heme(propylamine)(2-mercaptoethanol). These estimates indicate significantly weaker coupling to axial nitrogen when the sixth ligand is mercaptide sulfur, possibly because of an efficient metal dπ to ligand pπ or dπ orbital overlap that reduces the unpaired spin density in iron orbitals. The alternate possibility, that a mercaptide ligand causes a trans effect that reduces the overlap with axial nitrogen, cannot be ruled out without knowledge of the quadrupole coupling constant at that nitrogen.

For all the cases reported here, the anisotropy in the hyperfine coupling is small, with the smallest coupling term always occurring at g_{max}, in analogy to the hyperfine interaction reported for Fe(III) (imidazole)$_2$ porphyrins (Scholes et al., 1986). A point dipole coupling between metal electron and ligand nitrogen would be expected to have a *maximum* value along a line joining the nucleus and the unpaired electron (Hurst et al., 1985). The result that A_3 has the smallest value is consistent with a negative sign for a_{iso} and a coupling mechanism that involves no direct transfer of spin into the nitrogen ligands (Scholes et al., 1986). [In nitrogen radicals, unpaired spin in valence orbitals is known to give a positive value for a_{iso} (Carrington & McLachlan, 1967).] The large isotropic coupling contribution to the hyperfine interaction must then arise from a polarization of nitrogen electrons having some s orbital character, by the unpaired spin of iron (Scholes et al., 1986).

The trend in isotropic couplings from 4 to 5 MHz, with the amine weakest and the imidazole strongest, is inversely related to the order of ligand basicity and suggests that σ orbital interactions alone are not dominant in determining the strength of coupling to the coordinated nitrogen. An improvement in π overlap, however, between ligand orbitals and the metal t_{2g} orbitals containing unpaired spin, would result in stronger hyperfine interactions whatever the mechanism for spin localization in the ligand. A series of oxycobaltous TPP complexes also exhibit weaker axial ligand hyperfine interactions with stronger bases of the pyridine or imidazole type (Magliozzo et al., 1987) though in those complexes a different coupling mechanism may pertain. The stronger bases tend to destabilize the partially filled d_{z^2} orbital through which hyperfine coupling to axial nitrogen occurs by interaction with unpaired spin that resides mainly in a π^* orbital of bound oxygen. The quadrupole coupling constants for directly coordinated imino nitrogens obtained from simulations here are smaller than values for the free ligands (Ashby et al., 1978; Hsieh et al., 1977) because the lone pair acts as a donor to the empty d_{z^2} iron orbital (Johnson et al., 1991). The couplings here compare well with those reported in other spectroscopic studies of metal-coordinated ligands (Hsieh et al., 1977; Ashby et al., 1978, 1980; Rubenacker & Brown, 1980). The e^2Qq value for the proximal imidazole nitrogen in MbOH (2.3 MHz) is also in agreement with the value reported for this atom in high-spin aquo-metHb (2.24 MHz) (Scholes, 1982). This parameter might have been expected to be sensitive to the spin state of iron because of a change in overlap with the d_{z^2} orbital, which is empty in low-spin iron and partially filled in the high-spin case. The equivalence in the couplings here also demonstrates that this interaction is apparently insensitive to the formal charge of the heme complex. Furthermore, no trans effect is evident in the hydroxide complex compared to the aquo complex. A trans effect could cause a weakened donor interaction on the proximal side when the sixth ligand changes from neutral to negatively charged and would have been manifested in a larger e^2Qq value for the imidazole nitrogen in MbOH compared to the analogous site in metHb.

For the amino nitrogen of butylamine, no coupling data are available for the free ligand. The values for the axial amino nitrogen here, however, are consistent with those reported for the amino group in Cd(II) glycinato complexes (Ashby et al., 1980).

The values for the asymmetry parameter η were more difficult to accurately determine since the simulations were only moderately sensitive to this parameter. When the nuclear quadrupole interaction dominates the coupling interactions giving rise to modulations in the electron spin echo envelope, as found for the remote nitrogen coupling in Cu(II)–imidazole complexes (Mims & Peisach, 1979), the low-frequency components in spectra are very sensitive to the value of η (Jiang

[2] Simulations generated near the g_{mid} position of the EPR absorption usually contained more components than were seen in ESEEM spectra, which was an indication that a colinear axis arrangement of the hyperfine principal axis system with the g tensor was not quite accurate. For MbOH, a rotation of hyperfine axes (along with an adjustment of the values of the elements) reduced the intensity of extra components near 6–7 MHz and improved the simulation at $g = 2.17$, which then showed only a single line at 7 MHz. This procedure was not repeated for the model complexes since no important aspect of the interpretation of the results depends on these orientations.

[3] This value is calculated for ^{14}N from the ^{15}N hyperfine couplings given by Scholes et al. (1986) for Fe(III) coproporphyrin(imidazole)$_2$.

et al., 1990). In those cases, the asymmetry parameter can be more strictly fit to the data and would be more accurately determined. Nevertheless, the calculated η values for the axial nitrogens in the low-spin heme complexes are close to the ranges reported in nqr studies for the coordinated pyridine and amino nitrogens (Hsieh et al., 1977; Ashby et al., 1977, 1980; Rubenacker & Brown, 1980), but the value for imidazole in MbOH is somewhat low. The low value may be related to π bonding interactions that vary with the metal and ligand type. This issue cannot be resolved here without a survey of related complexes.

The parameters most easily related to the structure of the heme and Fe(III) TPP complexes are the nqi Euler angles. The frequencies and intensities of components in simulations were quite sensitive to the angle β, which as stated above, describes the orientation of the Q_{zz} axis of the quadrupole tensor relative to the g_z axis. Since nqr data are not available for iron complexes of the nitrogen ligands used here,[4] an assumption must be made about the orientation of the quadrupole tensor in the molecular framework of the coordinated ligand in order to obtain information about the orientation of the g tensor in these structures. The following discussion expands the outline of these ideas presented above.

Nqr studies addressed to a determination of the orbital occupancy of the coordinating imino or amino nitrogen "lone pair" orbital for a large number of Zn(II)- and Cd(II)-pyridine, imidazole, and amino acid complexes present information about the nqi principal axis directions. In the analysis of e^2Qq and η values for imino nitrogens, based on the Townes–Dailey model (Townes & Daily, 1949), the occupancies in the lobe of the sp^2 orbital coordinated to metal are less than two electrons but do not fall below ~1.8 electrons for pyridine and ~1.7 electrons for imidazole; the e^2Qq values associated with the nitrogens having these orbital populations were found to be 2–3 MHz for imidazole and 2.7–3.4 MHz for pyridine, with η values equal to 0.3–0.7 (imidazole) and 0.2–0.3 (pyridine) (Hsieh et al., 1977; Ashby et al., 1977, 1980; Rubenacker & Brown, 1980). The coupling constants are reduced from their values in the free ligands due to the electrophilic interaction between the Lewis acids (metals) and the nitrogen donor, though the values remain nearly three times larger than those reported for ammonium or iminium ions (Ashby et al., 1980; Edmonds et al., 1973). Furthermore, the relationships between e^2Qq and η show that the Q_{zz} axis of the imino nitrogen nqi tensor is directed along the lone pair orbital of the coordinated nitrogen and only shifts to another direction when the occupancies fall below ~1.53 (pyridine) and 1.63 (imidazole) electrons (with coupling constants reduced to ~1.5 MHz) (Hsieh et al., 1977; Ashby et al., 1978).

Similar results come from analysis of the nqr of coordinated *amino* groups in Zn(II)- and Cd(II)-amino acid and peptide complexes (e^2Qq = 2.6–3.0, η = 0.5–0.6, orbital occupancy ~1.7 electrons) (Ashby et al., 1980). For the amino nitrogen sp^3 hybrid orbital system, the largest component of the electric field gradient tensor lies in the plane between the hydrogens and can vary from coincident with the lone pair direction through an angle θ that places it along the nitrogen molecular z axis (θ from 35.3° to 0°) (Ashby et al., 1980; Edmonds et al., 1973). The η and e^2Qq values in the nqr experiments for the coordinated amino group are consistent with the Q_{zz} axis located close to the direction of the lone pair orbital in primary amines, as in the imino nitrogens.

The important feature to be emphasized from this discussion is that the range of e^2Qq values measured for the metal-coordinated nitrogen in all ligands studied by nuclear quadrupole resonance is in accord with the "lone pair" donor orbital defining the Q_{zz} axis. Since the coupling constants found here by simulation of the ESEEM spectra are within the same range, it is reasonable that Q_{zz} for axial ligands in the iron porphyrins again corresponds to the direction of the lone pair donor orbital. This orbital is axially directed along a σ bond to the iron d_{z^2} orbital, its direction corresponding to the normal to the porphyrin plane. A test of the orientation of Q_{zz} with respect to g_z in a low-spin heme in which g_z (g_{max}) lies near the heme normal (Helcke' et al., 1968; Hori, 1971) comes from a preliminary analysis of the proximal imidazole nitrogen coupling in Mb[$^{15}N_3^-$]. Simulation of ESEEM spectra for Mb[$^{15}N_3^-$] (not shown) demonstrates that Q_{zz} is nearly aligned with g_z (β = 15°). The small β values reported above demonstrate that g_{max} is nearly coincident with Q_{zz} and therefore corresponds to g_z in MbOH and in the model complexes.

Simulations were dependent on the other nqi Euler rotation angles, though no improvement in fits was achieved by changing them from values close to 0°. This result suggests that Q_{yy} is near to g_y (g_{mid}) in MbOH. The g_y axis lies perpendicular to the plane of the proximal imidazole nitrogen in MbN_3^- (Helcke' et al., 1968; Huynh et al., 1978). Q_{yy} also lies perpendicular to the plane of the ring for the imino nitrogens of pyridine and imidazole according to nqr axis assignments (Hsieh et al., 1977; Ashby et al., 1978), and, therefore, the g_y direction in MbOH is similar to g_y in MbN_3^-.

The nqi axis orientations for axial nitrogen in MbOH and the models are not in agreement with a recent ESEEM report on Mb(mercaptoethanol) (Flanagan & Singel, 1987). This low-spin complex has the axial ligand combination imidazole/RS^- and is an example of a species for which cancellation of nuclear Zeeman and hyperfine interactions occurs and for which ESEEM spectra are dominated by the nqi coupling frequencies (Peisach et al., 1979). "Anomalous" nqi axes were reported for the proximal imidazole nitrogen on the basis of the field-dependent variation in intensity of some low-frequency components in two-pulse ESEEM spectra (Flanagan & Singel, 1987). The results of spectral simulation for MbOH and the two models reported here do not reveal evidence for an anomalous nqi axis system in the directly coordinated nitrogens since simulations were unsatisfactory when the Euler angle β was assigned a large value. This angle would be large for an nqi system in which Q_{zz} deviated significantly from the lone pair orbital direction but where the lone pair was still directed along the heme normal.

Finally, the coupling parameters for the coordinated amino nitrogen in the Fe(III) TPP(butylamine)(OR^-) model do not reveal any features that distinguish it from an imino nitrogen, a result suggesting that an ESEEM study of a heme protein such as cytochrome *f* in its native form may not directly yield insights into the identity of axial ligands.

Porphyrin Nitrogen Couplings. The analysis of the porphyrin ^{14}N coupling parameters for MbOH was more difficult than the analysis of the imidazole coupling because of the multiplicity of lines in the native protein spectra (Figure 3). Since the spectra are characterized by very broad lines, the problem was approached in the following way: A simulation of the porphyrin pyrrole nitrogen components in the ESEEM spectrum of Fe(III) [^{14}N]TPP([^{15}N]pyridine)(OR^-) was

[4] The nqr results reported for the imino nitrogen of pyridine in the complex Fe(0) $(CO)_4$(pyridine) give an e^2Qq = 2.4 and η = 0.3 (Rubenacker & Brown, 1980). These values are within the range found for a set of complexes in which the largest component of the electric field gradient tensor is along the lone pair donor orbital of the sp^2 hybrid (see text).

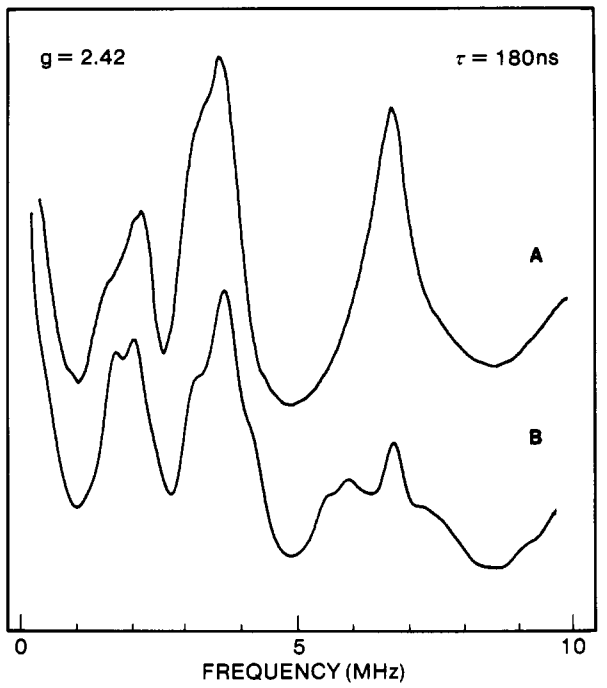

FIGURE 6: (A) ESEEM spectrum of the low-spin complex Fe(III) [^{14}N]TPP([^{15}N]pyridine)(OR^-). Experimental conditions: frequency, 8.8214 GHZ; magnetic field, 2600 Gauss; pulse power, 40 W. The axially coordinated nitrogen of [^{15}N]pyridine has a negligible contribution (see Figure 1, bottom). (B) Fourier transform of ESEEM simulation for four equivalent porphyrin nitrogens. Simulation parameters: A_x, A_y, A_z = 4.6, 5.1, 4.9 MHz; e^2Qq, 2.2 MHz; η = 0.2; nqi Euler angles α, β, γ = 0°, 48°, 0°.

achieved, treating the observed modulations as a single set of components from four equivalent nuclei (Figure 6). The parameters used for simulation of the pyrrole nitrogen data in this model are shown in Table I, section B. In order to accomplish a similar analysis for native MbOH, the pyrrole nitrogen contribution in ESEEM spectra had to be identified. Once the axial imidazole coupling frequencies were identified in spectra [^{15}N]heme MbOH, the additional components appearing in the native protein spectra could be assigned to porphyrin nitrogen couplings. The spectrum in Figure 3 contains some of these components at 7, 4.6, and 3.3 MHz. Simulations (not shown) giving approximate fits to the pyrrole components in spectra for native MbOH at three magnetic field settings were calculated by adjusting the parameters found to simulate spectra for the pyrrole nitrogens in Fe(III) TPP([^{15}N]pyridine)(OR^-). These parameters are also given in Table I, section B. The simulation of the MbOH pyrrole couplings is not straightforward because the ESEEM spectra are not simple sums of the separate modulations due to different nuclei. Furthermore, the axial ^{14}N coupling can not be removed in the protein case. Nevertheless, the highest frequency component arising from pyrrole couplings was resolved in ESEEM spectra at various experimental field settings, and the hyperfine coupling was readily calculated by assigning values for A_x, A_y, and A_z that simulated the field dependence of those components. The results show a less anisotropic coupling than that for the hyperfine interaction with axial nitrogens. For MbOH, the value of a_{iso}, 5.25 MHz, is nearly equal to the coupling found for the pyrrole nitrogens in Fe(III) [^{14}N]TPP([^{15}N]pyridine)(OR^-) (4.9 MHz). The value for MbOH is smaller than the average pyrrole coupling in high-spin metHb, 8 MHz (Scholes et al., 1982), and slightly smaller than the couplings reported for the porphyrin nitrogens in MbN_3^-, Fe(III) (imidazole)$_2$ porphyrins, and MbCN (6 MHz average) (Mulks et al., 1979; Scholes et al., 1986). The pyrrole couplings in MbOH and the TPP model are also weaker and much more isotropic than the pyrrole coupling in VOTPP (a_{iso} = 6.8 MHz, A_1, A_2, A_3 = 9.57, 2.90, 7.92 MHz) (Mulks & vanWilligen, 1981). The 20% smaller contact coupling and the small anisotropy for MbOH pyrrole nitrogens compared to the VOTPP case could arise from the different symmetry properties of the spin ground state for the metals in these complexes (d_{xy} for VO^+; d_{yz} in low-spin heme) and (or) from a structural difference. The smaller pyrrole coupling in MbOH compared to MbN_3^- suggests that the azide ligand can withdraw unpaired spin density from iron orbitals to a greater degree than the hydroxide ligand. This idea is consistent with some conclusions discussed below about the variation in crystal field splittings as a function of sixth ligand in heme complexes.

The quadrupole coupling constant for the pyrrole nitrogens in MbOH and the model (2.2 MHz) is comparable to the values reported from ENDOR experiments on a single crystal of high-spin aquo-metHb (Scholes et al., 1982) in which four sets of porphyrin components were resolved and assigned. The quadrupole coupling constants in metHb ranged from 2.00 to 2.16 MHz [these are calculated as 2 times that Q_{22} or Q_{max} values taken from Scholes et al. (1982)]. This coupling parameter, unlike the hyperfine coupling for the porphyrin nitrogens, was not expected to vary much with the spin state of the iron. The similarity between e^2Qq values for pyrrole and *imino* nitrogens as well as the similarity to the value in *N*-methylpyrrole (Arnold et al., 1968), where the nitrogen is covalently bound to a carbon, suggests that the formal charge carried by the porphyrinato macrocycle core (−2) is effectively neutralized in Fe(III) TPP and heme. The value for the coupling constant could be a reflection of both the essentially covalent nature of the iron–pyrrole bonds and the reduction of charge on the nitrogens by delocalization through the macrocycle system.

The value for the Euler angle β for the pyrrole nitrogens in MbOH (48°, Table I, section B) would be close to 90° if Q_{zz} were along the donor orbital σ bond direction in the heme plane. The 48° angle could result from an anomalous axis system in the pyrrole nitrogens similar to results reported for Cu(II) TPP (Brown & Hoffman, 1980).

The g Tensor in MbOH. If the assignment of *g* tensor axes used in simulation here, in a manner analogous to that for MbN_3^-, is valid then a crystal field analysis should give rhombic and axial crystal field splittings consistent with the nature of the low-spin complex containing hydroxide ion as the sixth ligand. The crystal field analysis (Taylor, 1977; Palmer, 1982) for low-spin iron is based on experimentally observed *g* values and allows calculation of the relative energies of the d_{xy}, d_{xz}, and d_{yz} orbitals of the t_{2g} set. An exemplary analysis considering all possibilities for assignment of g_{max}, g_{mid}, and g_{min} to g_z, g_y, and g_x, including negative *g* values, with the restriction that $g_z + g_y - g_x > 0$, has been presented for cytochrome *c* (Muhoberac, 1984). The product $g_xg_yg_z$ is suggested to be positive for low-spin heme complexes (Huynh et al., 1978), and, therefore, the *g* values here are taken to be positive. Axial (V_A) and rhombic (V_R) splittings calculated for MbOH using the *g* values reported under Materials and Methods and the assignment $g_z > g_y > g_x$, gives V_A/λ = 3.24 and V_R/λ = 5.47 with the d_{yz} orbital having the largest coefficient because it contains the unpaired spin (Figure 7). (λ is the spin-orbit coupling parameter). These splittings for MbOH are larger than splittings calculated in a similar way for MbN_3^- and MbCN (see below). Are the large splittings reasonable for the complex with an imidazole/hydroxide axial ligand combination?

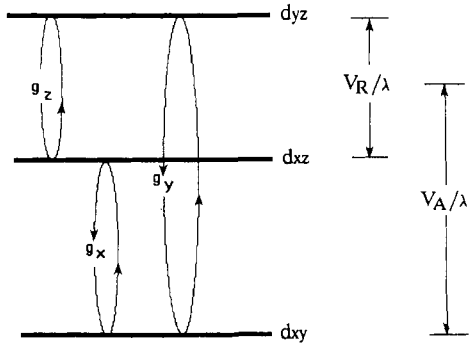

FIGURE 7: Relative energies of the three orbitals of the t_{2g} set arranged such that d_{yz} is highest and contains the unpaired electron. V_R/λ is the rhombic splitting and V_A/λ is the axial or tetragonal splitting. The three g values are defined according to the axes that relate the pairs of orbitals by simple rotation (see text).

The rhombic splitting is the difference in energy between the out-of-plane d_{xz} and d_{yz} orbitals. These orbitals are available for π bonding above and below the heme plane. The orbital symmetry of the proximal imidazole nitrogen, having a planar sp^2 valence shell, allows the lone pair orbital to orient a σ bond to the unoccupied iron d_{z^2} orbital (Johnson et al., 1991). Perpendicular to the σ bond is a nitrogen orbital of π symmetry that can overlap with d_{yz} and d_{xz}. The orientation of the imidazole plane, fixed by the polypeptide, allows π overlap with only one of the pair of $d\pi$ orbitals, and this interaction contributes to the difference in energy between the d_{xz} and d_{yz} orbitals. The symmetry of this proximal imidazole interaction is expected to be the same in all the low-spin forms of Mb. The spectroscopic differences occurring among the various low-spin forms having different sixth ligands may then be examined in terms of this ligand's interaction with the d orbital system, especially along the $d\pi$ planes. The oxygen of hydroxide ion, for example, has a symmetrical filled valence shell and no orbitals available for back donation from the iron. The hydroxide ligand cannot reduce the electron density in iron imposed by the other ligands, and its localized negative charge would tend to increase the energy of both d_{xz} and d_{yz}, relative to d_{xy}. The resulting axial and rhombic splittings would be expected to be large for the hydroxide species, as one in fact finds when these parameters are calculated using $g_{max} = g_z$, $g_{mid} = g_y$, and $g_{min} = g_x$.

The splittings for MbOH may be compared to the MbCN case, for which $V_R/\lambda = 0.92$ and $V_A/\lambda = 3.31$, are calculated using g values from single-crystal EPR measurements [$g_z = 3.45$, $g_y = 1.89$, and $g_x = 0.93$ (Hori, 1971)]. The very small rhombic splitting, according to the arguments just presented, could be ascribed to the good π acceptor property of the cyanide ligand, since the preferential removal of electron density from a filled $d\pi$ iron orbital would reduce the splitting imposed by the proximal imidazole π system. The back donation of electron density would result in a trend in axial couplings at the proximal imidazole ranging from large to small for MbOH compared to MbCN since the magnitude of that interaction is directly related to the unpaired spin density in iron. This interaction is in fact larger in MbOH ($a_{iso} = 5$ MHz) and significantly smaller in MbCN and MbN_3^- (not shown but estimated from preliminary simulations of ESEEM spectra for these other low-spin forms). The trend suggests that π acceptor ligands can give smaller rhombic splittings *and* smaller proximal imidazole couplings. Also, a large hyperfine coupling (5 MHz) is found by ENDOR spectroscopy for the nitrogen in the cyanide ligand in $MbC^{15}N$ (Mulks et al., 1979). This result is consistent with a large unpaired electron spin interaction at this site that could arise from transfer of electron density out of iron.

The alternate assignment of g values ($g_x > g_y > g_z$) for MbOH yields very small rhombic and axial splittings, seemingly inconsistent with the other low-spin forms and with the ideas discussed above. That axis labeling was arbitrarily made in an early report of the EPR spectrum of MbOH (Gurd et al., 1967) and was assigned in a more rigorous fashion in an LEFE study of various low-spin Mb and heme model complexes (Mims & Peisach, 1976). The interpretation of LEFE experiments suggested that the heme group in MbOH had an electronic structure quite different from other low-spin Mb species such that the spin-orbit coupling was larger than the crystal field splitting and the g tensor axis system in the molecular framework was reversed ($g_x > g_y > g_z$) compared, for example, to MbN_3^-. The assignment for MbOH, placing g_{max} (g_x) in the porphyrin plane, suggests that unpaired spin is localized in the plane of the porphyrin ring, presumably in the d_{xy} orbital. In VOTPP (d^1 metal ion), the unpaired spin is localized in the d_{xy} orbital (Smith, 1976). Therefore, the analogous electron configuration in the iron case, if it occurred in MbOH, might have been expected to result in a pyrrole nitrogen hyperfine coupling with significant anisotropy and an isotropic term close to 7 MHz, similar to the VOTPP example (Mulks & vanWilligen, 1981). The nearly isotropic hyperfine coupling of 5.25 MHz determined here for the porphyrin nitrogens in native MbOH argues against the localization of unpaired spin in the porphyrin plane, in the absence of large structural differences between these two metalloporphyrins. Furthermore, the results presented above show that simulations for the ESEEM of MbOH could be satisfactorily achieved with the g tensor assigned such that $g_z > g_y > g_x$, with Q_{zz} and g_z nearly aligned. (Simulations using $g_x > g_y > g_z$ were not satisfactory, though some values for e^2Qq and hyperfine coupling elements near to the values reported above did yield a simulation showing correspondences with data at $g = 2.4$ or 1.8, though not at both.) These results, taken with the reasonable way the crystal field analysis for MbOH given above is consistent with trends in the properties of sixth ligands, suggest that the g tensors in MbOH and MbN_3^- are similar. Can the LEFE results be interpreted without a reassignment of the g tensor axes for MbOH? A quantitative reexamination of the LEFE for MbOH is beyond the scope of this paper, but a discussion of the experiment and a plausible reinterpretation based on simple symmetry arguments is presented here.

Some background concerning the origin of the rhombic EPR signal for low-spin heme, illustrated by the concepts presented by Palmer (1985), helps to provide a framework for further discussion. The three d orbitals of the t_{2g} set are related to one another by rotations about the Cartesian axes. The magnetic field applied within the EPR absorption envelope can induce a "mixing" of a pair of these orbitals along an axis that relates them via simple rotation. For example, d_{xy} and d_{xz} are related through rotation about the x axis. The g value of the unpaired electron is shifted away from the free electron value by the coupling of its spin and orbital angular momenta, giving rise to three observed g values corresponding to three axes in the complex. The g_x resonance position, for example, lies where the EPR experimental conditions achieve resonance with the absorption of energy corresponding to a transition associated with the x molecular axis in the heme complex. This is illustrated schematically in the diagram (Figure 7). The g_z and g_y positions may be defined in similar ways. Single-crystal EPR results cited above have demonstrated that the g_z ($= g_{max}$) axis in fact corresponds well with the heme

Table II: LEFE Shift Parameters σ, Measured at g_{min} and g_{max} for MbN_3^- and MbOH[a]

	σ^b (g_{min})	σ (g_{max})
$Mb(N_3^-)$	0.4 ($E \parallel H_0$)[c] 2.3 ($E \perp H_0$)[d]	2.2 ($E \parallel H_0$) 0.37 ($E \perp H_0$)
MbOH[e]	3.2 ($E \parallel H_0$) 1.4 ($E \perp H_0$)	1.1 ($E \parallel H_0$) 3.6 ($E \perp H_0$)

[a] Data are taken from Mims and Peisach (1976). [b] In units of 10^{-9} $(V/cm)^{-1}$. [c] Applied electric field parallel to the external magnetic field. [d] Applied electric field perpendicular to the external magnetic field. [e] LEFE data for MbOH were reexamined for this work with essentially equivalent results (C. Bender and R. S. Magliozzo, unpublished results).

normal or the molecular z axis for MbN_3^- and that g_x lies in the porphyrin plane (Helcke' et al., 1968; Hori, 1971). Some additional arguments, required to describe the actual occurence of a g value above or below the free electron value, are omitted from the present discussion because the symmetry arguments alone give an easily understood model, given the relationship between molecular and g axes.

In the LEFE experiment, an electric field, E, is introduced at the sample, fixed either parallel or perpendicular to the external magnetic field, H_0. A LEFE shift parameter σ, related to a shift in g value, is measured at a series of magnetic field settings along the EPR spectrum [$\sigma \approx (\delta g/g)/E$]. The electronic polarization or perturbation that results from the large applied electric field (~10 kV) can affect ions in a crystal lattice or can polarize the metal and ligand wave functions (Mims, 1989). The end-of-spectrum shifts, i.e., the values of σ at g_{max} and g_{min} for frozen solutions of heme complexes, can be used to calculate parameters that are related to structural features of these species (Mims & Peisach, 1976). Table II shows the LEFE shifts for MbOH and MbN_3^- taken from Mims and Peisach (1976).

For MbN_3^-, when the electric field is applied parallel to H_0 at the low-field end of the EPR absorption, the perturbation along the axial direction causes a shift in g_z that, according to the symmetry arguments above, must arise from a change in the relative energies of d_{yz} and d_{xz}. Such a change in the rhombic splitting would not be expected to result from a perturbation directed along z because d_{yz} and d_{xz} are mutually perpendicular about the z axis. However, the azide ion in MbN_3^- is known to be bound to iron in a bent fashion (Stryer et al., 1964). Furthermore, the directly coordinated nitrogen could participate in a π bond to one of the out-of-plane d orbitals. Either of these considerations, that is either the bent bond for which negative charge resides in azide somewhere off the z axis or the π bonding interaction, would allow for a change in g_z from a change in d_{yz}–d_{xz} splitting upon application of the electric field parallel to H_0 at the low-field extreme. In other words, the perturbation along z may be translated into the x–y plane by virtue of the orientation of the azide ligand as well as (or) by the π overlap with out-of-plane d orbitals. The LEFE for MbN_3^- yields the result that at g_{max} larger shifts occur when E is parallel to H_0 (and perpendicular to H_0 at g_{min}) (Table II). This discussion ignores any effects from the proximal imidazole since these may be assumed to be equivalent, from the point of view of the symmetry arguments, for all low-spin forms.

For MbOH, the LEFE effects are opposite to those observed for MbN_3^-, such that at g_{max} larger shifts were observed when the electric field was *perpendicular* to H_0 (Table II). The oxygen of the hydroxide ligand in this complex has an electron configuration that results in a spherically symmetrical filled valence shell. Therefore, an electric field applied at the low-field end of the EPR spectrum, along the presumed g_z direction, would not be expected to induce a new d_{yz}–d_{xz} orbital splitting because no *new* asymmetry is created by polarization in that direction. The axial splitting, the spacing of d_{xy} relative to the $d\pi$ pair, could shift upon polarization along the heme normal (as would also have occurred in MbN_3^-), but such an effect does not directly alter g_z. The LEFE shifts for MbOH at g_{max}, if they still result from a shift in the d_{yz} or d_{xz} orbital energy, could occur instead through a polarization (perturbation) in the x–y plane, perpendicular to H_0 at g_{max}. If one considers the effect of polarization of the sixth ligand or iron orbitals along the z direction compared to some perturbation in the equatorial plane, it is the in-plane perturbation that can generate an effect on the d_{yz}–d_{xz} splitting when the sixth ligand is symmetrical about z (Figure 8). Then, for MbOH, a shift in g_z is predicted for polarization perpendicular to the z axis. This interpretation is consistent with the observed LEFE effects and does not require a "reversed" assignment of the g tensor axes for MbOH.

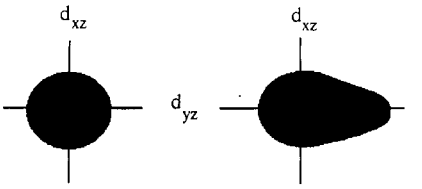

FIGURE 8: Schematic illustration of the interaction of a symmetrical sixth (axial) ligand with the mutually perpendicular planes containing the d_{yz} and d_{xz} orbitals. Application of an electric field perpendicular to the heme normal could cause a polarization of ligand orbitals along a plane such that the relative energies of d_{yz} and d_{xz} are altered. This change would yield a shift in g_z for MbOH.

Summary

The ESEEM spectra arising from iron–nitrogen electron nuclear couplings in low-spin Fe(III) porphyrin and heme complexes containing nitrogen and oxygen axial ligand pairs have been analyzed using angle selected simulation methods. The calculated nuclear quadrupole interaction parameters for the directly coordinated axial nitrogens are consistent with Q_{zz} located along the nitrogen lone pair orbital donor to iron. The assignment of g_z to the direction of the heme normal is consistent with the small angle found for the Euler rotation between the $g_{max} = g_z$ and Q_{zz} axes. The crystal field parameters calculated for MbOH, i.e., the axial and rhombic splittings between the orbitals of the t_{2g} set, are consistent with the behavior of the out-of-plane iron orbitals when back-donation to the axial sixth ligand is poor. The unusual LEFE effects for MbOH are also consistent with the nature of the filled shell symmetry of the oxygen in hydroxide.

Acknowledgments

We thank Drs. J. Cornelius, M. Colaneri, and A. Coffino for helpful discussions.

References

Ainscough, E. W., Addison, A. W., Dolphin, D., & James, B. R. (1978) *J. Am. Chem. Soc. 100*, 7585–7591.

Arnold, W., Dreizler, H., & Rudolf, H. D. (1968) *Z. Naturforsch. A23*, 301–306.

Ascoli, F., Rossi-Fanelli, M. R., & Antonini, E. (1981) *Methods Enzymol. 76*, 77–86.

Ashby, C. I. H., Cheng, C. P., & Brown, T. L. (1978) *J. Am. Chem. Soc. 100*, 6057–6067.

Ashby, C. I. H., Paton, W. F., & Brown, T. L. (1980) *J. Am. Chem. Soc. 102*, 2990–2998.

Brautigan, D. L., Feinberg, B. A., Hoffman, B. M., Margo-

liash, E., Peisach, J., & Blumberg, W. E. (1977) *J. Biol. Chem. 252*, 574–582.
Britt, R. D., & Klein, M. P. (1987) *J. Magn. Reson. 74*, 535–540.
Brown, T. G., & Hoffman, B. M. (1980) *Mol. Phys. 39*, 1073–1109.
Carrington, A., & McLachlan, A. D. (1967) in *Introduction to Magnetic Resonance*, pp 111–112, Harper & Row, New York.
Cornelius, J. B., McCracken, J., Clarkson, R. B., Belford, R. L., & Peisach, J. (1990) *J. Phys. Chem. 94*, 6977–6982.
Edmonds, D. T., Hunt, M. J., & Mackay, A. L. (1973) *J. Magn. Reson. 9*, 66–74.
Flanagan, H. L., & Singel, D. J. (1987) *J. Chem. Phys. 87*, 5606–5616.
Gadsby, P. M. A., Peterson, J., Foote, N., Greenwood, C., & Thomson, A. J. (1987) *Biochem. J. 246*, 43–54.
Gurbiel, R. J., Batie, C. J., Sivaraja, M., True, A. E., Fee, J. A., Hoffman, B. M., & Ballou, D. P. (1989) *Biochemistry 28*, 4861–4871.
Gurd, F. R. N., Falk, K.-E., Malmstrom, B. G., & Vanngard, T. (1967) *J. Biol. Chem. 242*, 5724–5730.
Helcke', G. A., Ingram, D. J. E., & Slade, E. F. (1968) *Proc. R. Soc. London, B. 169*, 275–288.
Hoffman, B. M., & Ballou, D. P. (1989) *Biochemistry 28*, 4861–4871.
Hori, H. (1971) *Biochim. Biophys. Acta 251*, 227–235.
Hsieh, Y.-N., Rubenacker, G. V., Cheng, C. P., & Brown, T. L. (1977) *J. Am. Chem. Soc. 99*, 1384–1389.
Hurst, G. C., Henderson, T. A., & Kreilick, R. W. (1985) *J. Am. Chem. Soc. 107*, 7294–7299.
Huynh, B. H., Emptage, M. H., & Munck, E. (1978) *Biochim. Biophys. Acta 534*, 295–306.
Jiang, F., McCracken, J., & Peisach, J. (1990) *J. Am. Chem. Soc. 112*, 9035–9044.
Johnson, C. R., Jones, C. M., Asher, S. A., & Abola, J. E. (1991) *J. Inorg. Chem. 30*, 2120–2129.
Lin, C. P., Bowman, M. K., & Norris, J. R. (1985) *J. Magn. Reson. 65*, 369–374.
Magliozzo, R. S., McCracken, J., & Peisach, J. (1987) *Biochemistry 26*, 7923–7931.
Martin, C. T., Scholes, C. P., & Chan, S. I. (1985) *J. Biol. Chem. 260*, 2857–2861.
McCracken, J., Peisach, J., & Dooley, D. M. (1987) *J. Am. Chem. Soc. 109*, 4064–4072.
Mims, W. B. (1972) *Phys. Rev. B6*, 3543–3545.
Mims, W. B. (1984) *J. Magn. Reson. 59*, 291–306.
Mims, W. B. (1989) in *Pulsed EPR: A New Field of Applications* (Keijzers, C. P., Reijerse, E. J., & Schmidt, J., Eds.) p 234, North Holland, Amsterdam.
Mims, W. B., & Peisach, J. (1976) *J. Chem. Phys. 64*, 1074–1091.
Mims, W. B., & Peisach, J. (1978) *J. Chem. Phys. 69*, 4921–4929.
Mims, W. B., & Peisach, J. (1979a) in *Biological Application of Magnetic Resonance* (Shulman, R. G., Ed.) pp 221–269, Academic Press, New York.
Mims, W. B., & Peisach, J. (1979b) *J. Biol. Chem. 254*, 4321–4323.
Muhoberac, B. B. (1984) *Arch. Biochem. Biophys. 233*, 682–697.
Mulks, C. F., & van Willigen, H. (1981) *J. Phys. Chem. 85*, 1220–1224.
Mulks, C. F., Scholes, S. P., Dickinson, L. C., & Lapidot, A. (1979) *J. Am. Chem. Soc. 101*, 1645–1654.
Palmer, G. (1985) *Biochem. Soc. Trans. 13*, 548–560.
Peisach, J., Mims, W. B., & Davis, J. L. (1979) *J. Biol. Chem. 254*, 12379–12389.
Peisach, J., Mims, W. B., & Davis, J. L. (1984) *J. Biol. Chem. 259*, 2704–2706.
Rigby, S. E. J., Moore, G. R., Gray, J. C., Gadsby, P. M. A., George, S. J., & Thomson, A. J. (1988) *Biochem. J. 256*, 571–577.
Riste, G., & Hyde, J. (1969) *J. Chem. Phys. 52*, 4633–4643.
Roberts, J. E., Brown, T. G., Hoffman, B. M., & Peisach, J. (1980) *J. Am. Chem. Soc. 102*, 825–829.
Rubenacker, G. V., & Brown, T. L. (1980) *Inorg. Chem. 19*, 392–398.
Scholes, C. P., Lapidot, A., Mascarenhas, R., Inubushi, T., Isaacson, R. S., & Feher, G. (1982) *J. Am. Chem. Soc. 104*, 2724–2735.
Scholes, C. P., Falkowski, K., Chen, S., & Bank, J. (1986) *J. Am. Chem. Soc. 108*, 1660–1671.
Siedow, J. N., Vickery, L. E., & Palmer, G. (1980) *Arch. Biochem. Biophys. 203*, 101–107.
Smith, K. M. (1976) *Porphyrins and Metalloporphyrins*, p 567, Elsevier, Amsterdam.
Stryer, L., Kendrew, J. C., & Watson, H. C. (1964) *J. Mol. Biol. 8*, 96–104.
Tang, S. C., Koch, S., Papaefthymiou, G. C., Foner, S., Frankel, R. B., Ibers, J. A., & Holm, R. H. (1976) *J. Am. Chem. Soc. 98*, 2414–2434.
Taylor, C. P. S. (1977) *Biochim. Biophys. Acta 491*, 137–149.
Teale, F. W. J. (1959) *Biochim. Biophys. Acta 35*, 543.
Townes, C. H., & Daily, B. P. (1949) *J. Chem. Phys. 17*, 782–796.